Geophysical Journal International

Geophys. J. Int. (2011) **184,** 1304–1310 doi: 10.1111/j.1365-246X.2010.04911.x

A scattering image of Campi Flegrei from the autocorrelation functions of velocity tomograms

L. De Siena,[1] E. Del Pezzo[2,3] and F. Bianco[2]

[1] *Institute for Geophysics, University of Münster, Correnstrasse* 24, *Münster* 48149, *Germany. E-mail: lucadesiena@uni-muenster.de*
[2] *Istituto Nazionale di Geofisica e Vulcanologia, Sezione di Napoli "Osservatorio Vesuviano", Via Diocleziano* 328, *Naples* 80124, *Italy*
[3] *Istituto Andaluz de Geofisica, Universidad de Granada, Granada, Spain*

Accepted 2010 November 29. Received 2010 November 25; in original form 2010 August 4

SUMMARY

We propose a new quantitative approach for the joint interpretation of velocity and attenuation tomography images, performed through the lateral separation of scattering and intrinsic attenuation. The horizontal *P*-wave scattering attenuation structure below Campi Flegrei Caldera (CFC) is imaged using the autocorrelation functions (ACF) of *P*-wave vertical velocity fluctuations. Cluster analysis (CA) is then applied to interpret the images derived from ACF and the available *P*-wave total attenuation images at 2000 m quantitatively. The analysis allows the separation of intrinsic and scattering attenuation on a 2-D plane, adding new geophysical constraints to the present knowledge about this volcanic area. The final result is a new, quantitative image of the past and present tectonic and volcanological state of CFC. *P*-wave intrinsic dissipation dominates in an area approximately located under the volcanic centre of Solfatara, as expected in a region with a large presence of fluids and gas. A north–south scattering attenuation region is mainly located below the zone of maximum uplift in the 1982–1984 bradiseismic crisis, in the sea side of the Pozzuoli bay, but also extending below Mt Nuovo. This evidence favours the interpretation in terms of a hard but fractured body, contoured by strong *S*-wave scatterers, corresponding to the Caldera rim: the region is possibly a section of the residual magma body, associated with the 1538 eruption of Mt Nuovo.

Key words: Probability distributions; Seismic attenuation; Seismic tomography; Statistical seismology.

1 INTRODUCTION

Traveltime tomography is the easiest way to obtain images of the Earth velocity structure, and hence deduce the physical properties of the propagation medium (Aki & Richards 1980). When velocity images are combined with total attenuation tomography images, new and sometimes critical features of the Earth medium are highlighted (Schurr *et al.* 2003; De Gori *et al.* 2005; Eberhart-Phillips *et al.* 2008). On the other hand, the joint interpretation of velocity and attenuation images is often biased by the difficulty of separating intrinsic and scattering attenuation (Sato & Fehler 1998; Del Pezzo *et al.* 2006). Although scattering *S*-wave tomography is able to highlight the presence and intensity of strong scatterers into the medium (Frederiksen & Revenaugh 2004; Tramelli *et al.* 2006), separate estimates of intrinsic and scattering *P*-wave attenuation at local scale are difficult to achieve from seismological data. Recordings of both local earthquakes and active shots are dominated by a mixture of shear and surface waves (Del Pezzo *et al.* 2006). Moreover, *P*-wave codas are as short as a few seconds, due to the small distances between sources and receivers. Consequently, the possibility of applying ordinary techniques, usually developed for *S* waves, such as fitting the *P*-coda energy envelope with theoretical multiple scattering models (Del Pezzo 2008) is precluded.

It is well known that the tectonic zones with the highest heterogeneity are volcanic areas. This is due to their peculiar topography and subsurface structure, made of unconsolidated, alternating layers of ash, pumice and volcanic rocks. The *P*-wave scattering properties of heterogeneous geological structures like volcanoes can be investigated inferring the attenuation properties from the distribution of the velocity fluctuations (Sato & Fehler 1998). At a scale lower than hundreds of metres, velocity fluctuations tend to be random, and can be described through the space autocorrelation function (ACF) and the corresponding power spectral density function (PSDF—the Fourier transform of the ACF; Chernov 1960; Aki & Chouet 1975; Sato & Fehler 1998). The ACFs provide a statistical measure of both the spatial scale and the magnitude of the heterogeneity characterizing the medium, whereas the PSDFs are mainly used to describe its spectral characteristics (Line *et al.* 1998). Different kinds of ACFs (Gaussian, exponential, von Kàrmàn) can be used to describe velocity fluctuations (e.g. Roth 1997). Anyway, the exponential and von Kàrmàn distribution better describe random depth-dependent velocity fluctuations in a stratified or volcanic medium (Holliger

et al. 1996; Shiomi *et al.* 1997; Shapiro & Hubral 1999). Sato & Fehler (1998) report a study of the normalized ACFs from velocity tomograms for the Jemez volcanic field, obtaining the correlation lengths in the vertical and horizontal directions. As a result of the strong stratification of the volcanic medium, vertical correlation lengths result shorter: velocity changes with depth result stronger, and can shade the presence of a horizontal velocity anomaly under the volcanic cone. ACFs can also be estimated from arrival-time data. Examples of traveltime fluctuations measured from active data are described by Roth (1997) and Line *et al.* (1998), who estimated the ACF parameters from seismic profiles. Traveltimes provide an unbiased approach, being unaffected by the smoothing effects introduced by damping factors and by the resolution problems generally affecting tomography procedures. On the other hand, traveltimes uncertainties in heterogeneous areas, if recorded from passive sources, are usually large, sometimes up to 20–30 per cent of the measured traveltimes. Moreover, although the ACFs obtained from traveltimes fluctuations can only image 2-D vertical profiles, velocity fluctuations provide an image of the lateral variations of scattering at a given depth.

We propose a quantitative approach to jointly interpret velocity and attenuation tomography images. We derive the velocity fluctuations directly from the *P*-wave velocity images obtained by Battaglia *et al.* (2008) below the Campi Flegrei Caldera (CFC), close to the city of Naples (Southern Italy). ACFs are calculated from the velocity fluctuations in the vertical direction to a depth of 4000 m starting from the surface. We derive the correlation length, a, and the mean square fractional fluctuations, ε^2, from the best fit of the experimental data with an exponential ACF. The inverse quality factor for *P* waves, Q_{PSc}^{-1} (Aki & Richards 1980; Sato & Fehler 1998) is deduced using the traveltime corrected Born approximation, and attributed to a depth of 2000 m. This method provides a 2-D scattering attenuation tomography of CFC; space-dependent intrinsic and scattering attenuation can be finally separated applying CA to the correlation lengths and Q_{PSc}^{-1} (obtained in this paper) and to the corresponding *P*-wave inverse total-Q, Q_{PT}^{-1}, recently obtained by De Siena *et al.* (2010).

2 THE STRUCTURE OF THE CAMPI FLEGREI CALDERA

The closeness to a densely inhabited area, with the high volcanic risk associated, makes CFC one of the most studied Calderas in the world. Geological, geophysical and volcanological data collected in the CFC produced a wide scientific bibliography. A summary of the most important geological and geophysical features of this area can be found in Zollo *et al.* (2008) and references therein: here we report only a brief outline. The Campi Flegrei Caldera is 6–7 km across; it formed about 15 ka BP during the Neapolitan Yellow Tuff eruption. Gravity (Berrino 1994), stratigraphical, volcanological, structural and petrological surveys (de Vita *et al.* 1999; Orsi *et al.* 2004), geochemistry (Caliro *et al.* 2007), active seismics (Zollo *et al.* 2008), active and passive velocity and attenuation tomography (De Lorenzo *et al.* 2001; Battaglia *et al.* 2008; De Siena *et al.* 2010) and borehole data (Orsi *et al.* 1996) indicate that the upper crust consists of volcanic rocks (mainly tuffs and lava layers) to a depth of 3000 m. Fig. 1(b) shows the main surface geological features and the local seismicity. The interpretation of both velocity and attenuation images are qualitatively sketched in Fig. 1(a), redrawn from De Siena *et al.* (2010) adding information from geochemistry. Basement rocks extending to 7500 m depth beneath the Caldera

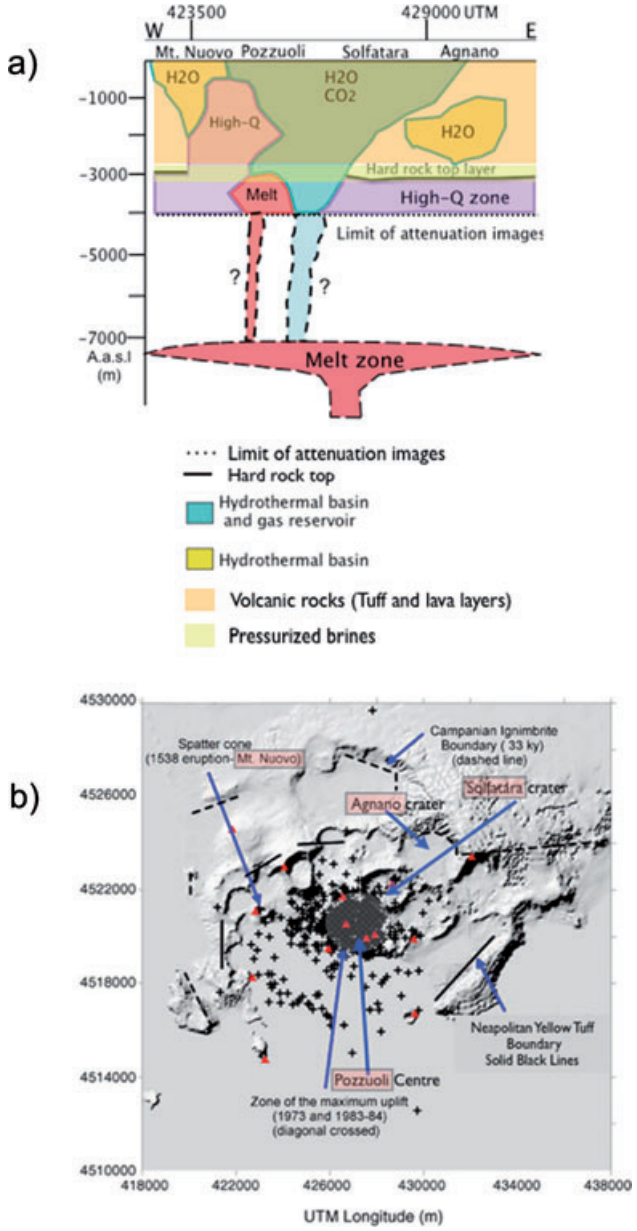

Figure 1. (a) Schematic cartoon of the geological structure of Campi Flegrei, deduced by velocity and attenuation tomography (Battaglia *et al.* 2008; De Siena *et al.* 2010). In the legend, dark colours refer to the interpretation deduced by tomography, whereas light colours summarize geochemical and geological interpretation. The melt zone at 7500 m depth has been deduced by a reflection study using explosive sources. The high-Q, violet body located in the western part of the sketch is characterized by high scattering attenuation, as described in the text. (b) Map of the area showing the main geological and geophysical signatures. Crosses mark the epicentre location of the local earthquakes. Blue arrows point to the zones characterized by important geological signatures, whose names are indicated in pink. Solfatara is a mud lake with visible residual volcanic activity (fumaroles, hot springs). Agnano is the crater formed during an important eruption occurred 10 000 yr ago. Mt Nuovo is the volcanic centre formed during the last eruption (1531 A.D.). The city of Pozzuoli is close to the area of maximum uplift during the 1983–1984 Bradiseismic crisis.

underlie a thermo-metamorphic layer at 3000–3500 m depth. A magma sill is laterally extended in the depth range 7500 data set and 8500 m beneath the whole Caldera (Zollo *et al.* 2008). The history of the ancient, peculiar activity of Campi Flegrei is reported

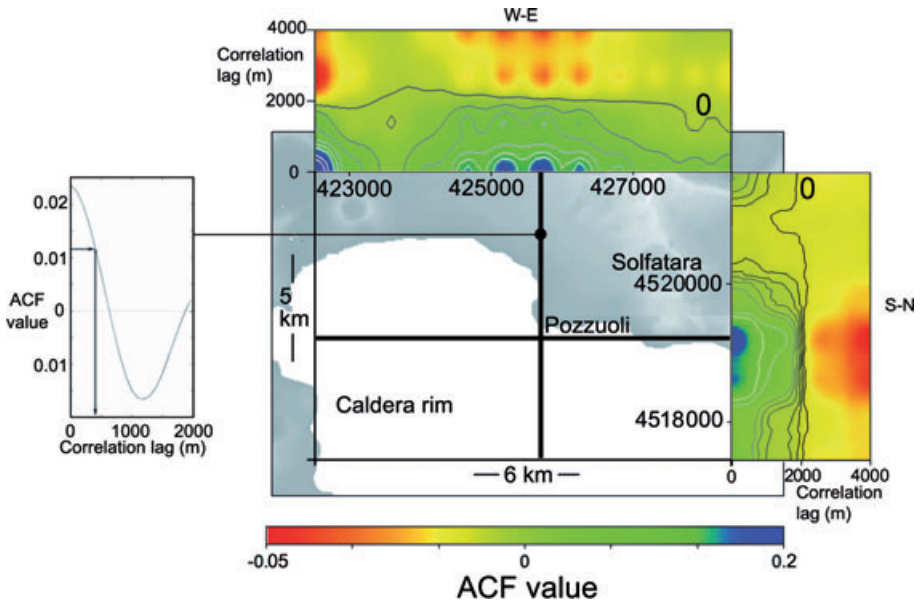

Figure 2. Map of the area (6 km × 5 km) selected for the analysis. Colour panels represent the ACFs measured for the W–E and S–N profiles marked with heavy black lines in the map. The colour scale corresponds to the ACF value. Isolines on the colour plot indicate the ACF isovalue. Coordinates are in UTM. The isoline marked with 0 corresponds to the correlation lag at which ACF crosses the lag-axis. An example of ACF is shown in the left part of the figure: the arrows show the correlation length, measured as the lag corresponding to the half-width of the ACF.

by Scandone *et al.* (2010) and references therein. The last eruption of this volcano (1538) was preceded and then followed during the time up to the present by many strong ground uplift episodes, called Bradiseism. The last episode occurred in 1982–1984, with a maximum uplift of more than 1.7 m in the centre of the Caldera, close to the city of Pozzuoli. Between the main uplift episodes the ground subsides relative to the sea level, even if a small Bradiseism (some centimetres) can still interrupt the subsidence. Any uplift (strong or minor) is always accompanied by seismic activity, consisting in volcano-tectonic earthquakes and in long-period local events. Several thousands of volcano-tectonic events (maximum magnitude of 4.2) accompanied the 1982–1984 uplift episode. This swarm constitutes the data set used in many tomography studies, as that of Battaglia *et al.* (2008) on which the present paper is based.

3 DATA SELECTION

Our starting data set consists of the 3-D distribution of *P*-wave velocity obtained by Battaglia *et al.* (2008) in an Earth volume of 18 × 18 × 9 km starting 0.5 km above sea level. In this work, they invert traveltime data from both active and passive sources simultaneously for the velocity model and the earthquake locations with an iterative, linearized perturbation technique. The passive data set is composed of 4472 *P* and 3268 *S* traveltimes, recorded during the 1984 bradiseismic crisis. traveltimes from active sources are measured from the recordings of 1528 shots at 70 sea-bottom receivers and 84 land stations during the SERAPIS experiment (Zollo *et al.* 2003) in 2001 September. In the joint inversion, both data sets contribute to the determination of V_P. The proper merging of the two data types provides overall high-resolution velocity models, which allow to reliably retrieve velocity anomalies over a large part of the area at a maximum resolution of 500 m in the centre of the Caldera. The average frequency of the data used in this tomography is 12 Hz whereas the average velocity is 6 km s^{-1} for the volumes we consider, which gives an average wavenumber of $k = 12\,\mathrm{km}^{-1}$.

We select the velocities on the base of the error and smoothing associated to them by the inversion. Seismic velocity estimates are provided at the vertexes of a 500 m step, 3-D grid: a 8 × 7 × 4 km cubic grid centred approximately at 2000 m depth, 1000 m southeast of the city of Pozzuoli is our starting data set. In this volume, the velocities are affected by an average 10 per cent error. The second selection is performed looking at the synthetic tests of Battaglia *et al.* (2008) (their figs 9, 10 and 12): we exclude a subvolume (recognized by Battaglia *et al.* 2008), where smoothing effects generated by the inversion process might be predominant, reducing the effective resolution. Our final data set is limited to a volume of 6 × 5 × 4 km, centred under the city of Pozzuoli (Fig. 2).

4 METHOD, DATA ANALYSIS AND RESULTS

Inhomogeneities in a random medium can be described by their ACF or, equivalently, by their PSDF (Chernov 1960; Aki & Chouet 1975). Correlation length, a, and mean square fractional fluctuations, ε^2, of the random field can be obtained from the ACF. These quantities provide a better understanding of the physical state of the low-depth crust than absolute velocity; moreover a *P*-wave lateral map of scattering attenuation can be obtained from them. In the following analysis, we will assume an exponential ACF to model depth-dependent random fluctuations of velocity in the volcanic area of CFC. Velocity fluctuations are obtained after the removal of a given trend. Removing the deterministic component, or detrending, is an important processing step in statistical analysis (Hu *et al.* 1996); anyway, the question of how and even whether de-trend space and time series has been the topic of some debate (Holliger *et al.* 1996; Dolan *et al.* 1998; Goff & Holliger 1999). In a laterally heterogeneous volcanic medium, characterized by an extremely various lithology, different depth-dependent velocity trends could be recognized even for lateral distances of a few hundred metres (Del Pezzo 2008). In the following, we will extract the velocity–depth functionality using simplicity constraints (Lilliefors 1967). The aim

of the de-trend is to obtain random fluctuations: CA is not be applied to the points where fluctuations are not random.

We denote with $V(x, y, z)$ the 3-D velocity model obtained through tomography, where *x, y, z* are the node of a 500 m step grid. For any couple of points (x^*, y^*) we consider the corresponding $V(x^*, y^*, z) = V^*(z)$. We assume that the average depth-dependent $V^*(z)$ can be fitted by a *N*th order polynomial $V^*(z) = a_0^* + a_1^* z + a_2^* z^2 + \ldots + a_N^* z^N$. In the above relationships, the symbol '*' stands for '*any*' point located at surface in the area under study. We use the Schwartz (or Bayesian) information criterion (*BIC*— Schwartz 1978) to determine the order of the polynomial to be removed from the velocity measures. The *BIC* is an asymptotic measure that must be minimized to select a particular parameter model among a class. It is given by

$$BIC = \frac{\phi^2}{\sigma_e^2} + \kappa \ln(n), \tag{1}$$

where ϕ^2 is the residual sum of squares from the model, σ_e^2 the error variance for normally distributed errors, κ is the number of model parameters and n the number of observations. For each polynomial order, we calculated *BIC* at any grid point, and then average *BIC*-values over the grid points. We obtain that a first-order polynomial ($k = 2$) minimizes the *BIC*. The best-fit coefficient for the polynomial are computed and used to de-trend the velocity model in the area

$$\tilde{v^*}(z) = V^*(z) - a_0^* - a_1^* z, \tag{2}$$

where $\tilde{v^*}(z)$ are the velocity fluctuation distribution with depth for any surface grid point (x^*, y^*). We apply the Lillie test (Lilliefors 1967) at a 5 per cent significance level to check both the randomness of the velocity fluctuations and the correctness of the de-trending process. The result is that $\tilde{v^*}(z)$ is a random distribution for more than 90 per cent of the (x^*, y^*) couples.

The exponential ACF is used to model the random fluctuations (Shapiro & Hubral 1999)

$$R(z) = \varepsilon^2 exp(-z/a), \tag{3}$$

where $R(0) = \varepsilon^2$ and z is the positive defined depth. We numerically calculate the normalized ACF, $R(\Delta z)$, defined by

$$R(\Delta z) = \langle \tilde{v}^*(z)\tilde{v}^*(z + \Delta z) \rangle , \tag{4}$$

where the brackets indicate spatial average and Δz is the correlation space-lag, positive for the increasing depth. Following the theory of elastic random fluctuations, we can write the relationship between Q_{PSc}^{-1}, ε^2 and a in the time-corrected Born approximation, assuming an exponential ACF:

$$Q_{PSc}^{-1}(k) = \frac{2\varepsilon^2 a^3 k^3 \left(4 - \nu_c^2\right)}{\left(1 + \nu_c^2 a^2 k^2\right)(1 + 4a^2 k^2)}, \tag{5}$$

where k is the wavenumber. The factor ν_c^2 is the cut-off wavenumber (e.g. Sato & Fehler 1998, p. 125), introduced to neglect the contribution of large forward scattering to correct the Born approximation at high frequencies (Wu 1982). For RMS fractional fluctuations below 20 per cent, various studies (Sato 1982; Frankel & Clayton 1986; Sato & Fehler 1998) propose a value of $\nu_c^2 = 1/4$. This value corresponds to neglecting scattering energy within a cone of angle 30° in the forward direction to calculate attenuation. Using this approximation, eq. (5) becomes

$$Q_{PSc}^{-1}(k) = \frac{15\varepsilon^2 a^3 k^3}{2(1 + a^2 k^2/4)(1 + 4a^2 k^2)}. \tag{6}$$

The spatial distribution of the ACF values is shown for two perpendicular profiles intersecting near the city of Pozzuoli in Fig. 2(a). For each point of the profiles, the ACF is measured (Fig. 2b) and represented through a colourscale. The correlation length a and ε^2 are estimated by the half width and maximum of the ACF (Roth 1997), respectively (Fig. 2, left panel). The space averaged correlation length is $a = 0.9 \pm 0.1$ km, as deduced by fitting a to an exponential distribution. The values of ε^2 measured at any couple of space coordinates constitute a sequence of independent and identically distributed random variables; its limit distribution is a generalized extreme value (GEV) distribution (Coles 2001). First, we first calculate the shape parameter, governing the cue of the generalized extreme value distribution, by fitting the distribution of ε^2 measured at each of the final 109 couples (x^*, y^*) to the theoretical GEV distribution. The best-fit gives a shape parameter of 0.4 ± 0.2 and a space-averaged value of ε^2 of 0.06 ± 0.02 (Fig. 3). Using eq. (5) we finally calculate the space-averaged inverse scattering quality factor for *P* waves, $\langle Q_{PSc}^{-1} \rangle = 0.0012 \pm 0.0004$.

5 COMPARISON WITH OTHER MEASURES THROUGH CLUSTER ANALYSIS

The $\langle Q_{PSc}^{-1} \rangle$ obtained with the methods described in the previous section is the first measure of scattering attenuation for *P* waves in this area. ACFs are computed on a number of points dependent on the actual resolution. In a volcanic heterogeneous area and at high frequencies, $\langle Q_{PSc}^{-1} \rangle$ is mainly dependent on ε^2 (Sato & Fehler 1998): we expect the lateral variations of Q_{PSc}^{-1} to be a good indicator of the lateral variation of scattering attenuation. K-means cluster analysis (Hartigan 1975) with Euclidean distance (CA) is applied to the patterns of correlation length, a (Fig. 4a), Q_{PSc}^{-1} (Fig. 4b) and Q_{PT}^{-1} (Fig. 4c), this last obtained at 2000 m depth by De Siena *et al.* (2010), having common resolution of (500 m).

The optimal number of clusters (three) has been determined using the Elbow Method (Hartigan 1975, Fig. 5) and the BIC criterion (Schwartz 1978). The results from CA are reported in Fig. 6. The orange cluster is generally characterized by high correlation length values, low Q_{PSc}^{-1} values and high total attenuation. The blue cluster is more clearly characterized by low a values, high Q_{PSc}^{-1} values and low total attenuation. Finally, the Green Cluster has intermediate values of these parameters.

6 DISCUSSION OF THE RESULTS

The Eastern part of the tomograms is mainly characterized by the orange cluster, with different a values, low Q_{PSc}^{-1} and high Q_{PT}^{-1}; its centre is located below the Solfatara volcanic crater. The attenuation mechanism in the Eastern part of CFC is dominated by intrinsic dissipation. This result is expected where the presence of high temperature fluids and/or gasses is evident at surface (e.g. Caliro *et al.* 2007). Temperatures measured at boreholes reach 300 °C at 1800 m depth, below Solfatara-Pisciarelli (see Fig. 1 for the map location of this site). Gas emissions show that this temperatures are due to the presence of an hydrothermal system whose base is located at a depth of about 1700 m (Vanorio *et al.* 2005). At this depth, the system is composed by pure water boiling at a temperature close to the critical point (Caliro *et al.* 2007), which causes strong attenuation of both *P* and *S* waves (De Siena *et al.* 2010). Some dis-uniformity in the composition is likely to exist beneath the other parts of Campi

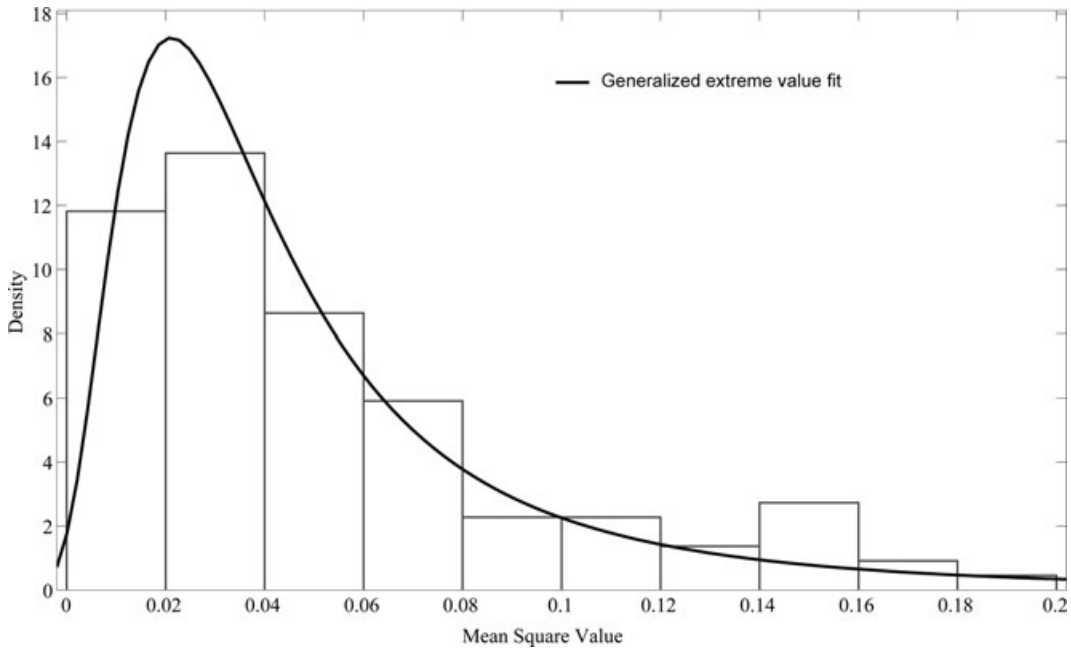

Figure 3. The fit of the probability density function (PDF) of the mean squared fractional fluctuations with a generalized maximum value PDF.

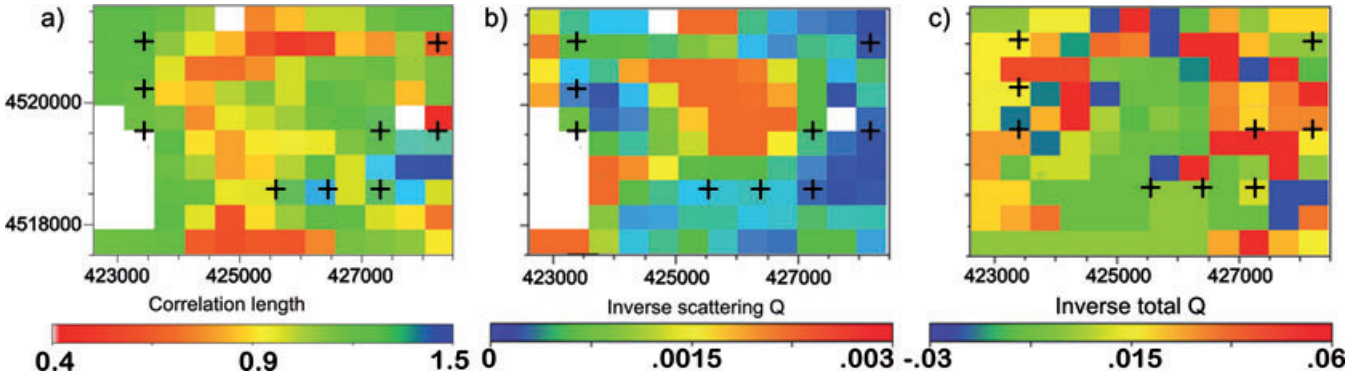

Figure 4. The spatial distribution of the correlation length (a), the *P*-wave inverse scattering (b) and total (c) quality factor at 2000 m depth, the latter obtained by De Siena *et al.* (2010). Coordinates are in UTM. Black crosses mark the position of strong *S*-wave scatterers (Tramelli *et al.* 2006). White blocks are not considered in the final analysis.

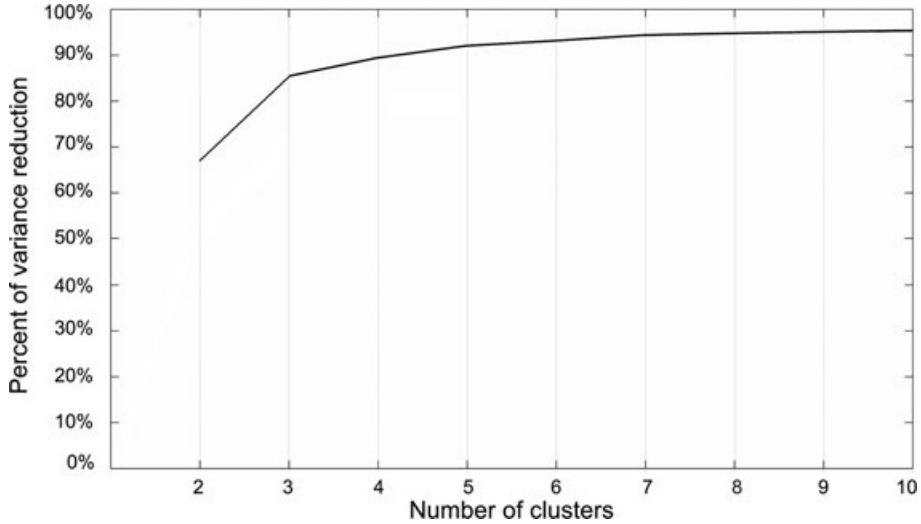

Figure 5. The percent of variance reduction versus the number of clusters. The number of cluster chosen is 3.

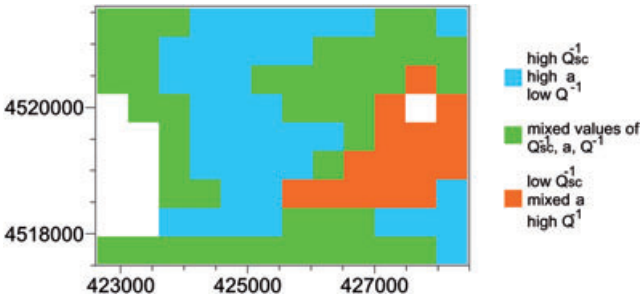

Figure 6. Result of the cluster analysis. Coordinates are in UTM. The colour of the three clusters (blue, green and orange) are represented with the corresponding physical parameters.

Flegrei at this depth, with the possible presence of deep brines, rich in H_3BO_3 (R. Moretti, personal communication).

The green cluster is not characterized by particular values of a, Q_{PSc}^{-1} and Q_{PT}^{-1}. By using the Elbow Criterium (Fig. 5), we set a reasonable limit to the information that the images can provide: the volumes characterized by the green cluster are the ones where a particular pattern could not be recognized and whose interpretation is therefore difficult.

The central part of the tomogram is mainly characterized by the blue cluster, extending from north towards south, and corresponding to high a, high Q_{PSc}^{-1} and low Q_{PT}^{-1}. To complete the interpretation for this particular area, we use the results of Tramelli *et al.* (2006), which obtained a scattering image of Campi Flegrei applying Nishigami's technique (Nishigami 1991) to *S*-wave codas of local earthquakes. The position of the strong S-to-S scatterers is marked by the black crosses on the three panels of Fig. 4. The strong scatterers are mainly located in correspondence with the zones of high Q_{PT}^{-1} and low Q_{PSc}^{-1} (Fig. 4b-c). Strong scatterers are not present in the north, central and southwestern part of CFC, where the pattern associated with the blue cluster is dominant (Fig. 6). This area is extended below the zone of Mofete-Monte Nuovo (where the last eruption in Campi Flegrei occurred) and centred below the area of maximum uplift during the volcanic crisis of 1982–1984. Most of this area is located in the sea side of the Pozzuoli bay. In the attenuation images, it mainly corresponds to the vertically elongated high-Q purple body in the western part of Fig. 1(a). This body is laterally extended towards east, approximately below the point of maximum uplift in the last bradiseismic crisis, and towards south, to the unique high attenuation anomaly present below 3000 m (De Siena *et al.* 2010). This result suggests the presence of a hard but fractured body, possibly the residual magma body associated with the 1538 eruption of Mt Nuovo. On the basis of stratigraphic data, integrated with geological, geochronological and geophysical constraints, Orsi *et al.* (1996) suggest that the conditions for magma to rise to surface at CFC are established only in the northeastern sector and in the area west of Mt Nuovo. In the central sector of CFC, the deformation must have occurred in a stress regime that has not allowed the establishment of such conditions. The presence of a zone of melt underneath the hard but fractured body could be important to model the dynamics of the 1982–1984 and following uplifts.

7 CONCLUSIONS

In volcanoes, velocity and attenuation patterns are highly discontinuous both laterally and in depth (Del Pezzo 2008). The interpretation of velocity and attenuation tomograms is often qualitative and hard to justify, at least without relying on observations coming from different geophysical fields (Hansen *et al.* 2004; De Gori *et al.* 2005; De Siena *et al.* 2010). The depth-dependent correlation lengths and inverse scattering quality factors deduced using ACFs vary from place to place towards the seismotectonic and volcanological settings of the region under study. The application of CA to this quantities, derived from velocity tomography, and to the inverse total quality factor, provides a quantitative, unsupervised image of the medium, giving a new insight into the past and present state of CFC.

ACKNOWLEDGMENTS

A number of colleagues have helped with suggestions for the improvement of this material. Haruo Sato is gratefully acknowledged for his deep review of the manuscript in its early stage, giving invaluable suggestions for its improvement. We would also thank Roberto Moretti, INGV, Lucia Zaccarelli, IPGP, Christine Thomas, University of Münster and two anonymous reviewers for their suggestions and corrections, and the RISSC-Lab., for providing velocity data. This study has been partly supported by the DPC-INGV Projects UNREST and Speed, granted by INGV and the Civil Defense of Italy and partly by the PRIN 2007 Project granted by Italy's Ministry of Education and Scientific Research.

REFERENCES

Aki, K. & Chouet, B., 1975. Origin of coda waves: source, attenuation, and scattering effects, *J. geophys. Res.,* **80,** 3322–3342.

Aki, K. & Richards, P., 1980. *Quantitative Seismology - Theory and Methods*, W.H. Freeman, San Francisco.

Battaglia, J., Zollo, A., Virieux, J. & Dello Iacono, D., 2008. Merging active and passive data sets in traveltime tomography: the case study of Campi Flegrei Caldera (Southern Italy), *Geophys. Prospect.,* **56,** 555–573.

Berrino, G., 1994. Gravity changes induced by height-mass variations at the Campi Flegrei Caldera, *J. Volc. Geotherm. Res.,* **61**(3–4), 293–309.

Caliro, S., Chiodini, G., Moretti, R., Avino, R., Granieri, D., Russo, M. & Fiebig, J., 2007. The origin of the fumaroles of la solfatara (Campi Flegrei, South Italy), *Geochimica et Cosmogonica Acta,* **71,** 3040–3055.

Chernov, L.A., 1960. *Wave Propagation in a Random Medium*, McGraw-Hill, New York.

Coles, S., 2001. *An Introduction to Statistical Modeling of Extreme Values*, Springer Series in Statistics, Springer, Berlin.

De Gori, P., Chiarabba, C. & Patan, D., 2005. Qp structure of Mount Etna: constraints for the physics of the plumbing system, *J. geophys. Res.,* **110**(B05303), doi:10.1029/2003JB002875.

De Lorenzo, S., Gasparini, P., Mongelli, F. & Zollo, A., 2001. Thermal state of the Campi Flegrei Caldera inferred from seismic attenuation tomography, *J. Geodyn.,* **32,** 476–486.

De Siena, L., Del Pezzo, E. & Bianco, F., 2010. Campi Flegrei seismic attenuation image: evidences of gas reservoirs, hydrothermal basins and feeding systems, *J. geophys. Res.,* **115**(B09312), doi:10.1029/2009JB006938.

de Vita, S. *et al.*, 1999. The Agnano Monte Spina eruption (4100 years bp) in the restless Campi Flegrei Caldera (Italy), *J. Volc. Geotherm. Res.,* **91**(2–4), 269–301.

Del Pezzo, E., 2008. Seismic wave scattering in volcanoes, in *Earth Heterogeneity and Scattering Effects of Seismic Waves, Vol. 50 of Advances in Geophysics*, chap. 13, pp. 353–369, Elsevier, Amsterdam.

Del Pezzo, E., Bianco, F. & Zaccarelli, L., 2006. Separation of Qi and Qs from passive data at Mt Vesuvius: a reappraisal of the seismic attenuation estimates, *Phys. Earth planet. Inter.,* **159,** 202–212.

Dolan, S., Bean, C. & Riollet, B., 1998. The broadband fractal nature of heterogeneity in the upper crust from petrophysical logs, *Geophys. J. Int.,* **132,** 489–507.

Eberhart-Phillips, D., Chadwick, M. & Bannister, S., 2008. Three-dimensional attenuation structure of central and southern south island,

New Zealand, from local earthquakes, *J. geophys. Res.,* **113**(B05308), doi:10.1029/2007JB005359.

Frankel, A. & Clayton, R.W., 1986. Finite difference simulations of seismic scattering implications for the propagation of short-period seismic waves in the crust and models of crustal heterogeneity, *J. geophys. Res.,* **91,** 6465–6489.

Frederiksen, A.W. & Revenaugh, J., 2004. Lithospheric imaging via teleseismic scattering tomography., *Geophys. J. Int.,* **159,** 978–990.

Goff, J.A. & Holliger, K., 1999. Nature and origin of upper crustal seismic velocity fluctuations and associated scaling properties: combined stochastic analyses of KTB velocity and lithology logs, *J. geophys. Res.,* **104**(B6), 13 169–13 182.

Hansen, S., Thurber, C.H., Mandernach, M., Haslinger, F. & Doran, C., 2004. Seismic velocity and attenuation structure of the East Rift Zone and South Flank of Kilauea Volcano, Hawaii, *Bull. seism. Soc. Am.,* **94,** 1430–1440.

Hartigan, J.A., 1975. *Clustering Algorithms*, Wiley Series in Probability and Mathematical Statistics, John Wiley & Sons, New York.

Holliger, K., Kanamori, H. & Clayton, R.W., 1996. Upper-crustal seismic velocity heterogeneity as derived from a variety of P-wave sonic logs, *Geophys. J. Int.,* **125,** 813–829.

Hu, K., Ivanov, P.C., Chen, Z., Carpena, P. & Stanley, H.E., 1996. Effect of trends on detrended fluctuation analysis, *Phys. Rev. E,* **62,** 011114, doi: 10.1103/PhysRevE.64.011114.

Lilliefors, H., 1967. On the Kolmogorov-Smirnov test for normality with mean and variance unknown, *J. Am. Stat. Assoc.,* **62,** 399–402.

Line, C., Hobbs, R.W. & Snyder, D.B., 1998. Estimates of upper-crustal heterogeneity in the baltic shield from seismic scattering and borehole logs, *Tectonophysics,* **286,** 171–183.

Nishigami, K., 1991. A new invertion method of coda waveforms to determine spatial distribution of coda scatterers in the crust and uppermost mantle, *Geophys. Res. Lett.,* **12**(18), 2225–2228.

Orsi, G., Vita, S.D. & Vito, M.D., 1996. The restless resurgent Campi Flegrei Caldera (Italy): constraints on its evolution and configuration, *J. Volc. Geotherm. Res.,* **74,** 179–214.

Orsi, G., Vito, M.D. & Isaia, R., 2004. Volcanic hazard assessment at the restless Campi Flegrei Caldera, *Bull. Volc.,* **66,** 514–530.

Roth, M., 1997. Statistical interpretation of traveltime fluctuations, *Phys. Earth planet. Inter.,* **104,** 213–228.

Sato, H., 1982. Amplitude attenuation of impulsive waves in random media based on travel time corrected mean wave formalism, *J. acoust. Soc. Am.,* **71,** 559–564.

Sato, H. & Fehler, M.C., 1998. *Seismic Wave Propagation and Scattering in the Heterogeneous Earth*, Springer and Verlag, New York, NY.

Scandone, R., D'Amato, J. & Giacomelli, L., 2010. The relevance of the 1198 eruption of Solfatara in the Phlegrean Fields (Campi Flegrei) as revealed by medieval manuscripts and historical sources, *J. Volc. Geotherm. Res.,* **189**(1–2), 202–206, doi:10.1016/j.jvolgeores.2009.09.012.

Schurr, B., Asch, G., Rietbrock, A., Trumbull, R. & Haberland, C.H., 2003. Complex patterns of fluid and melt transport in the central Andean subduction zone revealed by attenuation tomography, *Earth planet. Sci. Lett.,* **215,** 105–119.

Schwartz, G., 1978. Estimating the dimension of a model, *Ann. Stat.,* **6**(2), 461–464.

Shapiro, S.A. & Hubral, P., 1999. *Elastic Waves in Random Media, Fundamentals of Seismic Stratigraphic Filtering*, Springer, Berlin.

Shiomi, K., Sato, H. & Ohtake, M., 1997. Broad-band power-law spectra of well-log data in Japan, *Geophys. J. Int.,* **130,** 57–64.

Tramelli, A., Pezzo, E.D., Bianco, F. & Boschi, E., 2006. 3D scattering image of the Campi Flegrei Caldera (southern Italy). New hints on the position of the old Caldera rim, *Phys. Earth planet. Int.,* **155,** 269–280.

Vanorio, T., Virieux, J., Capuano, P. & Russo, G., 2005. Three-dimensional tomography from P wave and S wave microearthquake travel times and rock physics characterization of the Campi Flegrei Caldera, *J. geophys. Res.,* **110**(B03201), doi:10.129/2004JB003102.

Wu, R.S., 1982. Attenuation of short period seismic waves due to scattering, *Geophys. Res. Lett.,* **9,** 9–12.

Zollo, A. et al., 2003. Evidence for the buried rim of Campi Flegrei Caldera from 3-d active seismic imaging, *Geophys. Res. Lett.,* **30**(19), doi:10.1029/2003GL018173.

Zollo, A., Maercklin, N., Vassallo, M., Dello Iacono, D., Virieux, J. & Gasparini, P., 2008. Seismic reflections reveal a massive melt layer feeding Campi Flegrei Caldera, *Geophys. Res. Lett.,* **35**(L112306), doi:10.1029/2008GL034242.